

## **Shock-like free-surface perturbations in low-surface-tension, viscous, thin-film flow exterior to a rotating cylinder**

E. J. Hinch, M. A. Kelmanson and P. D. Metcalfe

*Proc. R. Soc. Lond. A* 2004 **460**, 2975-2991

doi: 10.1098/rspa.2004.1327

---

### **Email alerting service**

Receive free email alerts when new articles cite this article - sign up in the box at the top right-hand corner of the article or click [here](#)

---

To subscribe to *Proc. R. Soc. Lond. A* go to: <http://rspa.royalsocietypublishing.org/subscriptions>

---

## Shock-like free-surface perturbations in low-surface-tension, viscous, thin-film flow exterior to a rotating cylinder

BY E. J. HINCH<sup>1</sup>, M. A. KELMANSON<sup>2</sup> AND P. D. METCALFE<sup>1</sup>

<sup>1</sup>*Department of Applied Mathematics and Theoretical Physics,  
Centre for Mathematical Sciences, University of Cambridge,  
Wilberforce Road, Cambridge CB3 0WA, UK*

<sup>2</sup>*Department of Applied Mathematics, University of Leeds,  
Leeds LS2 9JT, UK (mark@maths.leeds.ac.uk)*

*Received 5 August 2003; accepted 19 March 2004; published online 7 July 2004*

Continuing from the work of Hinch & Kelmanson (2003 *Proc. R. Soc. Lond. A* **459**, 1193–1213), the lubrication approximation is used to investigate the drift and decay of free-surface perturbations in the viscous flow exterior to a circular cylinder rotating about its horizontal axis in a vertical gravitational field. Non-dimensional parameters corresponding to gravity,  $\gamma = \rho g \bar{h}^2 / 3\omega\mu a$ , and surface tension,  $\alpha = \sigma \bar{h}^3 / 3\omega\mu a^4$ , are used to characterize the flow, where  $\omega$  and  $a$  are respectively the angular velocity and radius of the cylinder,  $\mu$ ,  $\rho$ ,  $\sigma$  and  $\bar{h}$  are respectively the kinematic viscosity, density, surface tension and mean film thickness of the fluid, and  $g$  is the acceleration due to gravity. Within the parameter hierarchy  $\gamma^2 \ll \alpha \ll \gamma \ll 1$ , Hinch & Kelmanson (2003) discovered a complex interaction between rotation, gravity and surface tension, leading to a four-time-scale cascade over which drift and decay of free-surface perturbations occur. However, when  $\alpha = o(\gamma^2)$ , the low-harmonic asymptotics of Hinch & Kelmanson (2003) cannot represent the shock-like solutions manifest in numerical simulations.

Accordingly, the case of vanishingly small surface tension is investigated herein, and the resulting shock-like solutions are analysed. When the surface tension is identically zero, the resulting Hamiltonian problem may be solved explicitly via the method of characteristics, action-angle variables and strained-coordinate asymptotic expansions, which reveal a shock-formation time-scale of  $\omega^2 \mu^3 a^3 / \rho^3 g^3 \bar{h}^6$ . The strained (fast) time-scale  $\tau$ , which can be deduced *a priori* via action-angle variables, is consistent with that obtained via the independent asymptotic approach of Hinch & Kelmanson (2003), and the (slow) shock time-scale  $T = 30\gamma^3 t$  is derived and confirmed via spectral numerical integrations of the full lubrication approximation with vanishingly small, non-zero surface tension.

With  $\beta \equiv \alpha / 30\gamma^3 \ll 1$ , a shock thickness of order  $O(\beta^{1/3})$  is discovered, and the leading-order transient in the surface elevation is found to satisfy a Kuramoto–Sivashinsky evolution equation, which is solved via multiple scales for the extreme cases  $\beta \ll 1$  and  $\beta \gg 1$ , and numerically otherwise. A universal scaling of the transient results is discovered which gives good agreement with the quasi-steady shock solution, even when the transient shock thickens in response to its decreasing amplitude.

Depending upon critical values of  $\alpha/\gamma^2$ ,  $\beta$  and  $\gamma$ , the transient solution is discovered to decay in one of only four possible sequences comprising one or more of  $T^{-1}$ ,  $T^{-1/2}$  and  $\exp(-81\alpha\gamma^2t)$ . Physical data indicate that all four decay sequences are observable in practice.

**Keywords:** viscous fluid mechanics; free-surface flow; lubrication approximation; asymptotic expansions; computer algebra

## 1. Introduction

Hinch & Kelmanson (2003) use multiple-time-scale asymptotics to consider the well-studied problem (first considered by Moffatt (1977) and Pukhnachev (1977)) of the time-dependent evolution of the free surface of a thin film of viscous fluid adhering to the exterior of a rotating horizontal circular cylinder in a vertical gravitational field. Non-dimensional parameters corresponding to gravity and surface tension, respectively, are used to characterize the flow,

$$\gamma = \frac{\rho g \bar{h}^2}{3\omega\mu a} \quad \text{and} \quad \alpha = \frac{\sigma \bar{h}^3}{3\omega\mu a^4}, \quad (1.1)$$

in which  $\omega$  and  $a$  are respectively the angular velocity and radius of the cylinder,  $\mu$ ,  $\rho$ ,  $\sigma$  and  $\bar{h}$  are respectively the kinematic viscosity, density, surface tension and mean film thickness of the fluid, and  $g$  is the acceleration due to gravity. The numerical factors in (1.1) absorb those in the free-surface-elevation equation given by Pukhnachev (1977).

Specifically, Hinch & Kelmanson (2003) consider the non-dimensional evolution equation (representing mass conservation) and initial condition

$$\partial_t h + \partial_\theta h - \partial_\theta(\gamma h^3 \cos \theta - \alpha h^3 \partial_\theta(\partial_\theta^2 h + h)) = 0, \quad h(\theta, 0) = 1, \quad (1.2)$$

for the film thickness  $h(\theta, t)$  exterior to a rotating cylinder, where  $\gamma$  and  $\alpha$  are given by (1.1). The initial condition represents a uniform initial film thickness, the film height  $h$  having been non-dimensionalized with respect to the mean film thickness  $\bar{h}$ , and time  $t$  with respect to  $\omega^{-1}$ . Moreover, the parameters in (1.1) are such that the decay from the initial uniform state is to a final, nearly uniform film.

Within the hierarchy considered by Hinch & Kelmanson (2003),

$$\gamma^2 \ll \alpha \ll \gamma \ll 1, \quad (1.3)$$

the existence of four distinct time-scales over which different physical mechanisms act is deduced: first, there is the fast process of rotating with the cylinder on the (referential) time-scale 1; second, surface tension squeezes the free surface to a cylindrical shape on the time-scale  $\alpha^{-1}$ ; after this time, disturbances to the steady state take the form of an eccentricity of the cylindrical shape of the free surface which drifts in phase on the third time-scale of  $\gamma^{-2}$  and decays exponentially on the fourth and slowest time-scale of  $\alpha^{-1}\gamma^{-2}$ —specifically, at the rate  $81\alpha\gamma^2$ . These asymptotic findings are all corroborated by Hinch & Kelmanson (2003) via numerical evidence, both for the hierarchy (1.3) and for  $\alpha$  as small as  $O(\gamma^2)$ .

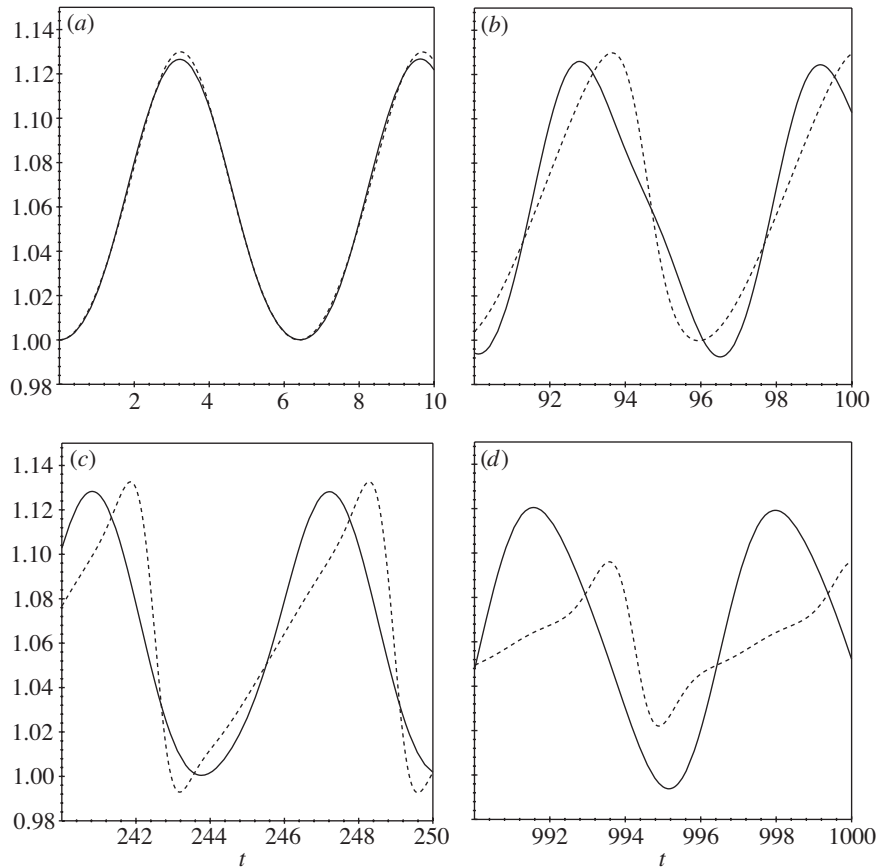


Figure 1. Breakdown of low-harmonic asymptotics when  $\alpha = o(\gamma^2)$  ( $\gamma = 5.32 \times 10^{-2}$  and  $\alpha = 4.8 \times 10^{-5} \simeq \gamma^{3.39}$ ). Free-surface elevation  $h(\theta, t)$  plotted at station  $\theta = 0$ . Four-term two-time-scale expansion (—) compared with spectral results (---). (a)  $0 \leq t \leq 10$ , (b)  $90 \leq t \leq 100$ , (c)  $240 \leq t \leq 250$ , (d)  $990 \leq t \leq 1000$ . Spectral results obtained with: 128 modes; adaptive time-stepping; absolute and relative error tolerances respectively  $10^{-10}$  and  $10^{-7}$ ; mass conserved to machine accuracy. Fast Fourier transforms performed using FFTW of Frigo & Johnson (1998) (see <http://www.fftw.org>).

If, however, the hierarchy (1.3) is violated, i.e.  $\alpha = o(\gamma^2)$ , Hinch & Kelmanson (2003) demonstrate, but do not analyse, the breakdown of their asymptotics. Figure 1 shows results for the case  $\alpha \simeq \gamma^{3.39}$ ; the numerical results obtained via a mass-conserving spectral method differ appreciably from the asymptotic results as  $t$  increases. In particular, figure 1c reveals that shock-like solutions form (for  $\gamma = 5.32 \times 10^{-2}$  and  $\alpha = 4.8 \times 10^{-5}$ ) at approximately  $t = 250$ , and figure 1d reveals that the amplitude decay is far greater than the expected  $\exp(-81\alpha\gamma^2t)$  predicted by the large-time asymptotics. This observation is addressed in some detail in § 4.

In § 2, analysis is undertaken of the limiting theoretical case of zero surface tension, which naturally leads to post-shock overturning waves. Although this is not physically possible in the thin-film limit because of the dissipative and diffusive terms in the lubrication approximation for the film height, analysis of this case is useful

in obtaining theoretical pre-shock information and, in particular, an estimate of the shock time itself. In the absence of surface tension, the hyperbolic first-order lubrication approximation can be analysed in terms of a Hamiltonian which admits an action-angle formulation, whose essential role is in determining the fast-time drift of the system *a priori* to an arbitrarily high order. This is in stark contrast to the analysis of Hinch & Kelmanson (2003), in which higher-order corrections to the drift are obtained at the expense of considerable algebraic manipulation as the asymptotic-series solution develops through orders of  $\gamma$ . With the drift rate known, the problem is solved using strained-coordinate asymptotic expansions, and a theoretical estimate is obtained for the shock time; this estimate dictates the slow time-scale over which shock formation occurs. All results are verified by convincing agreement with the results obtained independently via a spectral numerical method.

In §3 the drift rate and shock time-scale  $T$  of §2 admit a two-time-scale asymptotic analysis of the lubrication approximation. The parameter  $\beta = \alpha/30\gamma^3$ , a measure of the balance between surface tension and gravity-induced drift leading to shock formation, is introduced. Assuming  $\beta$  to be  $O(1)$ , equivalently  $\alpha = O(\gamma^3)$ , multiple-time-scale analysis reveals that the shock evolution is governed by a Kuramoto–Sivashinsky equation (KSE).

In §4 the case when  $\beta \ll 1$  is discussed. Then, an implicit solution of the KSE is possible, thereby providing an insight into the hierarchy of the relative magnitude of terms in the KSE. Non-uniformity is shown to arise in the asymptotic analysis of §3 when  $\alpha = O(\gamma^6)$ ; then, the shock structure and evolution are no longer dictated by the KSE. Hence, by  $\beta \ll 1$  is meant  $O(\gamma^3) \gg \alpha \gg O(\gamma^6)$ . Despite this restrictive relation between  $\alpha$  and  $\gamma$ , the limit  $\beta \rightarrow 0$  is admissible and a two-time-scale analysis of the KSE reveals that disturbances initially decay as  $T^{-1}$ , whereafter a changeover to a  $T^{-1/2}$  decay is observed at later times; such asymptotic analysis is corroborated by numerical integrations of the KSE.

In §5 the case  $\beta \gg 1$ , when no shocks form, is considered. A large- $\beta$  asymptotic analysis reveals that disturbance amplitudes decay as  $T^{-1/2}$ , and the common  $T^{-1/2}$  decay of the large- $T$ –small- $\beta$  and large- $T$ –large- $\beta$  regimes is explained. A small-time comparison of the precise form of the  $T^{-1/2}$  decay rate with the exponential decay rate observed by Hinch & Kelmanson (2003) suggests a transition region when  $\alpha \sim \gamma^2/2$ , an interesting consequence of which is the restriction  $\gamma \ll 1/60$ . A heuristic theory is proposed to account for the transition, and the theory verified by numerical solution of the governing equation (1.2).

In §6, the quasi-steady shock structure is analysed when  $\beta \ll 1$ ; it is deduced that the shock thickness is  $(2\beta/A)^{1/3}$ , where  $A$  is the shock amplitude. Numerically determined transient solutions of the full governing thin-film equation are rescaled and compared with the quasi-steady shock structure. The rescaling permits such a comparison to be made irrespective of (small)  $\alpha$  and  $\gamma$ , and the comparison reveals good universal agreement within the main rise of the shock, any discrepancies occurring away from the shock due to the large-time spreading of the numerical solution as its amplitude decays.

Finally, in §7, the findings of the earlier sections are reconsidered to show that only four possible sequences of decay transition, for varying  $\alpha$  and  $\gamma$ , are possible. By considering physical data for five different fluids, examples are found which indicate that all four discovered decay sequences are indeed observable in practice.

## 2. Vanishing surface tension: shock formation

Since solutions of (1.2) as  $\alpha \rightarrow 0$  are required, the limiting case  $\alpha \equiv 0$  is first considered. Then, (1.2) may be solved by the method of characteristics from the coupled ordinary differential equations

$$\frac{d\theta}{dt} = 1 - 3\gamma h^2 \cos \theta, \quad \theta(0) = \theta_0, \quad (2.1)$$

$$\frac{dh}{dt} = -\gamma h^3 \sin \theta, \quad h(0) = 1. \quad (2.2)$$

Before undertaking the solution of the characteristic equations, note that the system (2.1) and (2.2) admits the Hamiltonian

$$H(\theta, h) \equiv h - \gamma h^3 \cos \theta, \quad (2.3)$$

so that action-angle variables  $(J, \phi)$  are readily determined (via the MAPLE algebraic manipulator) to be

$$J = H + \frac{3}{2}\gamma^2 H^5 + \frac{165}{8}\gamma^4 H^9 + O(\gamma^6 H^{13}), \quad (2.4)$$

$$\phi = \theta + 3\gamma J^2 \sin \theta + \frac{15}{4}\gamma^2 J^4 \sin 2\theta + \gamma^3 J^6 \left(\frac{63}{2} \sin \theta + 7 \sin 3\theta\right) + O(\gamma^4 J^8). \quad (2.5)$$

Further, the angular velocity  $(\partial H/\partial J)$  is found to be

$$\Omega = 1 - \frac{15}{2}\gamma^2 J^4 - \frac{675}{8}\gamma^4 J^8 + O(\gamma^6 J^{12}), \quad (2.6)$$

and, noting from (2.3) that  $H(\theta(0), h(0)) = 1 - \gamma \cos \theta_0$ , (2.4) and (2.6) give the angular velocity explicitly as

$$\Omega(\theta_0) = 1 - \frac{15}{2}\gamma^2 + 30\gamma^3 \cos \theta_0 - \left(\frac{1215}{8} + \frac{45}{2} \cos 2\theta_0\right)\gamma^4 + O(\gamma^5). \quad (2.7)$$

Thus, the mean angular velocity taken over all the initial data  $\theta_0 \in [0, 2\pi)$  is

$$\Omega_0 = 1 - \frac{15}{2}\gamma^2 - \frac{1215}{8}\gamma^4 + O(\gamma^6). \quad (2.8)$$

The action-angle determination of  $\Omega(\theta_0)$  thus provides us with a means of averting secularity in the solutions for  $\theta$  and  $h$  to any pre-specified order; without this *a priori* knowledge, the expansion (2.7) would have to be constructed laboriously, as information was gleaned term-by-term from the increasingly higher-order (and increasingly more complicated) terms in multiple-scale expansions for  $\theta(t, \gamma^2 t)$  and  $h(t, \gamma^2 t)$ , as per Hinch & Kelmanson (2003). With the angular velocity determined, the coupled characteristic equations (2.1) and (2.2) are rescaled with respect to the drift time-scale  $\tau = \Omega(\theta_0)t$  and then solved interactively by expanding  $\theta(\theta_0, \tau)$  and  $h(\theta_0, \tau)$  as asymptotic series in powers of  $\gamma$ . We find

$$\begin{aligned} \theta(\theta_0, \tau) = & \theta_0 + \tau - 3(s_{11} - s_{10})\gamma + \frac{3}{4}(s_{22} - 2s_{21} + s_{20} + 10s_{01})\gamma^2 \\ & - \frac{1}{4}\{15(s_{12} + 10s_{11} - 9s_{10} - 2s_{1-1}) + (s_{33} - 3s_{32} + 3s_{31} - s_{30})\}\gamma^3 \\ & + O(\gamma^4), \end{aligned} \quad (2.9)$$

$$h(\theta_0, \tau) = 1 + (c_{11} - c_{10})\gamma + 3(1 - c_{01})\gamma^2 + \frac{15}{4}(3c_{11} - 4c_{10} + c_{1-1})\gamma^3 + O(\gamma^4), \quad (2.10)$$

wherein  $c_{mn} = \cos(m\theta_0 + n\tau)$  and  $s_{mn} = \sin(m\theta_0 + n\tau)$ . Equations (2.9) and (2.10) reveal that, during one cylinder rotation commencing at time  $t_0 > 0$ ,  $\theta$  and  $h$  change respectively by

$$\begin{aligned}\Delta\theta &= 2\pi - 15\pi\gamma^2 + 15\pi(3\cos(\theta_0 + t_0) + 4\cos\theta_0)\gamma^3 + O(\gamma^4), \\ \Delta h &= 15\pi\sin(\theta_0 + t_0)\gamma^3 + O(\gamma^4).\end{aligned}$$

Hence there is an  $O(\gamma^2)$  uniform drift counter to the rotation of the cylinder. By contrast, the perturbations at  $O(\gamma^3)$  in both  $\theta$  and  $h$  are dependent upon the initial data  $\theta_0$  and therefore represent a non-uniform drift which gives rise to shock formation at that order. Note too the first appearance of the reflected modes  $c_{1-1}$  and  $s_{1-1}$  at  $O(\gamma^3)$  in (2.9) and (2.10).

In the calculation of subsequent results, the expansions (2.9) and (2.10) were obtained up to and including terms of order  $O(\gamma^5)$ . Figure 2 shows the evolution of the free surface as calculated via characteristics, action-angle variables and numerical integration for the specific case  $\gamma = 0.05$ ; the action-angle and characteristic results differ imperceptibly at the presented resolution.† Superimposed over the crosses and circles is the (non-overturning) spectral solution of the full evolution equation (1.2) in the case  $\alpha = 1.0 \times 10^{-9}$ . It is evident that both the characteristic and action-angle solutions accurately represent the solution to large times in the non-overturning region; specifically, the absolute error in the Hamiltonian  $H(\theta(\theta_0, \Omega t), h(\theta_0, \Omega t))$  lies within the interval  $[10^{-8}, 10^{-5}]$  when  $t = 1000$ . But the most striking and useful observation is from figure 2*b*, which shows that the characteristic and action-angle solutions are accurate—on comparison with the spectral solution of (1.2)—even as the gradients increase and the shock begins to form (here, at  $t \simeq 250$ ). Although the post-shock overturning characteristic and action-angle solutions of figure 2*c, d* no longer have physical meaning, they are still accurate in those regions which have not passed into the shock. In other words, even after the shock has formed in the case  $0 < \alpha \ll 1$ , the  $\alpha \equiv 0$  characteristic solution is accurate away from the shock region.

The accuracy of (2.9) and (2.10) demonstrates that the shock time can be obtained theoretically. The surface gradient  $(\partial h/\partial\theta)_t$  becomes infinite at a time  $t_s$  given by

$$t_s = -\left(\frac{\partial\theta}{\partial\theta_0}\right)_\tau \left(\Omega'(\theta_0)\left(\frac{\partial\theta}{\partial\tau}\right)_{\theta_0}\right)^{-1} = \frac{1}{30\gamma^3\sin\theta_0} + O(\gamma^{-2}), \quad (2.11)$$

so that, in dimensional terms, the shock-formation time is  $\omega^2\mu^3a^3/30\rho^3g^3\bar{h}^6$ . When  $\gamma = 0.05$ , (2.11) reveals that the first point into the shock emanates from approximately (because of the  $O(\gamma^{-2})$  error)  $\theta_0 = \pi/2$  when  $t = 1/30\gamma^3 \simeq 267$ . At this value of  $\gamma$ , the full asymptotic series (2.9) and (2.10) reveals that the first point into the shock emanates from  $\theta_0 \simeq 0.598\pi$  when  $t \simeq 230$ ;  $t_s$  is *ca.* 16% too large. When  $\gamma$  is reduced to 0.01, (2.11) gives  $t_s \simeq 33\,933$  and  $\theta_0 = \pi/2$ , whereas the asymptotic series gives  $t \simeq 33\,148$  and  $\theta_0 \simeq 0.521\pi$ ; now,  $t_s$  is too large by only 2%.

† A greatly enlarged version of figure 2 reveals that the (action-angle) crosses do not exactly centre on the corresponding (characteristic) circles: a result of the proximity to the convergence limit, particularly as  $t$  increases, of the series reversion process used to extract the physical angle  $\theta$  from the variable  $\phi$ .

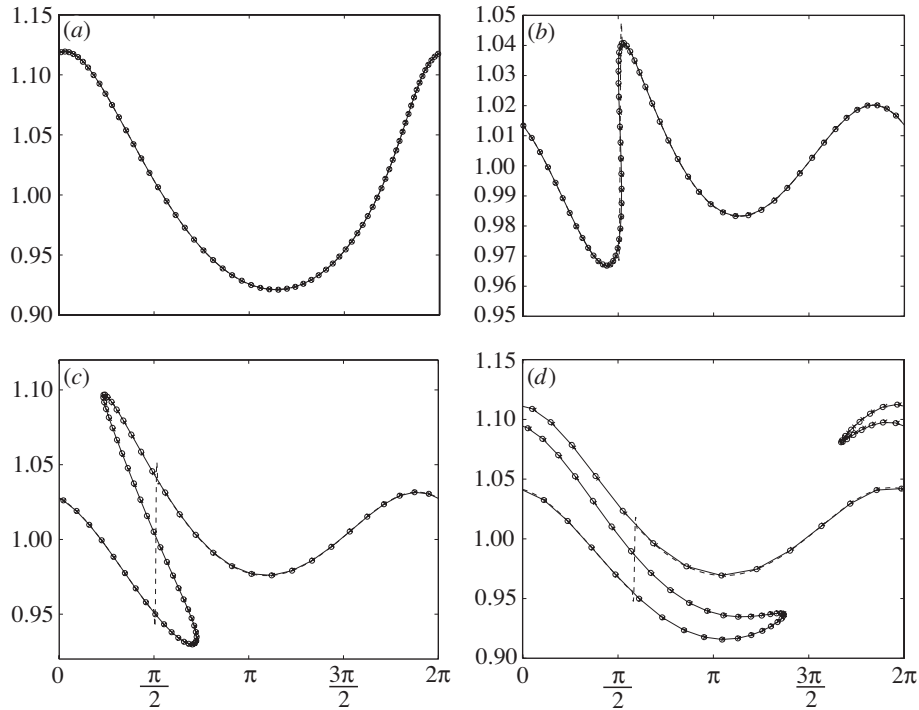


Figure 2. Free-surface profiles for  $\gamma = 0.05$  relative to initial frame  $\theta_0 \in [0, 2\pi)$  at (a)  $t = 100$ , (b)  $t = 250$ , (c)  $t = 500$ , (d)  $t = 1000$ .  $\circ$ ,  $\alpha = 0$  characteristic solution from (2.9) and (2.10);  $\times$ ,  $\alpha = 0$  action-angle solution extracted from (2.4) and (2.5); —,  $\alpha = 0$  numerical integration of (2.1) and (2.2); - - -,  $\alpha = 1.0 \times 10^{-9}$  spectral integration of full partial differential equation (1.2).

### 3. Shock-like solutions: the KSE

Non-shock secularities arising purely through drift are precluded by means of the coordinate transformations  $\xi = \theta$  and  $\eta = \theta - \tau = \xi - \Omega_0 t$ , where  $\Omega_0$  is the mean angular velocity taken over all initial data, as introduced in (2.8). A suitable two-time-scale expansion is then

$$h(\theta, t) = h_s(\theta) + h_u(\xi, \eta, T) = h_s(\theta) + \sum_n \gamma^n H_n(\xi, \eta, T), \quad (3.1)$$

wherein the slow time-scale is  $T = 30\gamma^3 t$  as suggested by (2.11),  $h_u(\xi, \eta, T)$  is the unsteady component of the solution and  $h_s(\theta)$ , the steady component of the solution, is an extended version of the steady-state equation (5.1) of Hinch & Kelmanson (2003), expanded for small  $\alpha$ :

$$h_s(\theta) = 1 + \gamma c_1 + \gamma^2 \left( \frac{3}{2} c_2 - 9\alpha s_2 \right) + \gamma^3 \left( \frac{9}{2} c_1 + 3c_3 - 9\alpha [3s_1 + 11s_3] \right) \\ + \gamma^4 \left( \frac{65}{4} c_2 + \frac{55}{8} c_4 - \alpha [435s_2 + \frac{1419}{2} s_4] \right) + O(\gamma^2 \alpha^2, \gamma^5), \quad (3.2)$$

where  $c_m = \cos m\theta$  and  $s_m = \sin m\theta$ . Spatial and temporal derivatives now transform in (1.2) as  $\partial_\theta \rightarrow \partial_\xi + \partial_\eta$  and  $\partial_t \rightarrow -\Omega_0 \partial_\eta + 30\gamma^3 \partial_T$ , and the shock-formation time is  $T = 1$ . In order to obtain physical (non-overtopping) solutions, the surface tension

$\alpha$  must balance the  $30\gamma^3$  slow-time-scale drift towards shocks introduced in §2. We therefore introduce the parameter

$$\beta \equiv \frac{\alpha}{30\gamma^3}, \quad (3.3)$$

wherein the proposed balance leads us presently to assume  $\beta = O(1)$ , although the limiting cases  $\beta \ll 1$  and  $\beta \gg 1$  are indeed admissible and are discussed respectively in §§4 and 5. Having substituted (3.3) and expansion (3.1) into equation (1.2), determination of  $H_n$  is straightforward for  $n = 1, 2, 3$ . At  $O(\gamma)$  we have

$$H_1(\xi, \eta, T) = f_1(\eta, T), \quad f_1(\eta, 0) = -\cos \eta. \quad (3.4)$$

Determination of  $f_1$  effectively solves the problem. By design, its evolution equation will arise at order  $O(\gamma^4)$ . At  $O(\gamma^2)$  we have

$$H_2(\xi, \eta, T) = 3 \sin \xi \partial_\eta f_1 + 3 \cos \xi f_1 + f_2(\eta, T), \quad f_2(\eta, 0) = \frac{3}{2} \cos 2\eta. \quad (3.5)$$

$H_2$  represents the oscillatory perturbation of  $H_1$  arising from the changing orientation of gravity relative to the point  $\theta(t)$  during one cylinder rotation. Specifically,  $\gamma H_2$  can be interpreted as a combination of phase and amplitude (respectively first and second terms on the right-hand side of (3.5)) corrections to  $H_1$ .

At  $O(\gamma^3)$  we have

$$\left. \begin{aligned} H_3(\xi, \eta, T) &= \frac{15}{2} \cos 2\xi f_1 + 3 \cos \xi f_1^2 + \frac{33}{4} \sin 2\xi \partial_\eta f_1 + 3 \cos \xi f_2 \\ &\quad - \frac{9}{4} \cos 2\xi \partial_\eta^2 f_1 + 3 \sin \xi \partial_\eta f_2 + 6 \sin \xi f_1 \partial_\eta f_1 + f_3(\eta, T), \\ f_3(\eta, 0) &= -\frac{9}{4} \cos \eta - 3 \cos 3\eta. \end{aligned} \right\} \quad (3.6)$$

While many of the terms in  $\gamma^2 H_3$  represent corresponding phase and amplitude corrections to  $H_1 + \gamma H_2$ , the second, fifth and seventh terms on the right-hand side of (3.6) do not. Containing first and second harmonics,  $H_3$  represents the perturbation due to drift which, by construction of  $\eta$  (which contains the mean angular velocity  $\Omega_0$ ), is uniform and does not give rise to secularity. However, secularity (in  $\xi$ ) arises as expected—indeed, required—in the  $O(\gamma^4)$  problem for  $H_4$ , and its annihilation requires that the as-yet-unknown function  $f_1(\eta, T)$  satisfies the nonlinear evolution equation

$$\partial_T f_1 - f_1 \partial_\eta f_1 + \beta \partial_\eta^2 (\partial_\eta^2 f_1 + f_1) = 0, \quad f_1(\eta, 0) = -\cos \eta, \quad (3.7)$$

which is a specific case of the KSE (Holmes 1995, p. 279). Thus, the leading-order transient perturbation satisfies a KSE with constant coefficients, which should be contrasted with the  $\theta$ -dependent equation (1.2). Note further that (3.7) reveals that  $\beta = O(1)$  has the physical interpretation that surface tension is then of sufficient magnitude to balance the  $O(\gamma^3)$  non-uniform drift discovered in §2.

#### 4. Vanishingly small surface tension: the case $\beta \ll 1$

The fact that the dominant transient  $f_1$  satisfies the KSE (3.7) is a direct consequence of the balance  $\alpha = O(\gamma^3)$ . If surface tension were reduced to  $\alpha = O(\gamma^{3+m})$ ,  $m > 0$ ,  $\beta$  cannot be redefined as  $O(\alpha/\gamma^{3+m})$ , since (3.7) would not arise at  $O(\gamma^4)$ . Rather, when  $\alpha = O(\gamma^{3+m})$ , definition (3.3) must be retained and  $\alpha$  considered to be of order  $O(\gamma^m) \ll 1$ , where it is to be noted that there is a resultant restriction on  $m$ .

Equation (3.1) ceases to be valid when  $H_1 \sim \gamma H_2$ . By construction, the  $f_n$  in (3.4)–(3.6) are  $O(1)$ , so that  $H_1 = O(1)$  and  $H_2 = O(\partial_\eta f_1) = O(\gamma/\alpha^{1/3})$ , the last estimate being based upon the shock thickness  $\beta^{1/3}$  determined in §6. Hence, the expansion for  $h_u$  ceases to be uniformly valid when  $1 = O(\gamma^2/\alpha^{1/3})$ , i.e.  $\alpha = O(\gamma^6)$ . Thus, if  $m \geq 3$ , the shock structure is no longer determined by (3.7), and by  $\beta \ll 1$  we mean  $O(\gamma^6) \ll \alpha \ll O(\gamma^3)$ . Thus an analysis of (3.7) in the limit  $\beta \rightarrow 0$  is justified only if  $\gamma^3 \ll \beta$ .

An asymptotic expansion for the solution of (3.7) is proposed in the form

$$f_1(\eta, T) = \sum_{n=0}^{\infty} \beta^n F_n(\eta, T), \quad (4.1)$$

wherein  $T = 30\gamma^3 t$  is the shock-formation time-scale dictated by (2.11) and, by construction, all  $F_n$  are of order  $O(1)$ . The  $O(1)$  problem is

$$\partial_T F_0 - F_0 \partial_\eta F_0 = 0, \quad F_0(\eta, 0) = -\cos \eta, \quad (4.2)$$

with the implicit solution

$$F_0(\eta, T) = -\cos(\eta + TF_0(\eta, T)). \quad (4.3)$$

It is evident from the discussion of the characteristic solutions of §2 and the shock structure in §6 that (4.3) is the solution of (3.7) provided  $\eta$  is not within  $O(\beta^{1/3})$  of the shock. The implicit solution (4.3) has a shock forming at  $T = 1$  and  $\eta = \pi/2$ , the amplitude of the shock thereafter eventually decaying as  $\pi/T$  since, if  $C_0 \equiv \cos(\eta + F_0 T)$  and  $S_0 \equiv \sin(\eta + F_0 T)$ , implicit differentiation of (4.3) gives

$$\partial_T F_0 = \frac{S_0 F_0}{1 - S_0 T} \quad \Rightarrow \quad F_0 \sim \frac{b_0(\eta)}{T}, \quad T \gg 1,$$

where  $b_0(\eta)$  is determined as  $\frac{1}{2}\pi - \eta$ . For large  $T$ , the last points into the shock are  $\eta = -\frac{1}{2}\pi$  and  $\eta = \frac{3}{2}\pi$ , i.e.  $|b_0(\eta)| \rightarrow \pi$ . Thus, between  $T = O(1)$  and  $T = O(\beta^{-1}) \gg 1$ ,  $|F_0|$  (and so  $|f_1|$ ) decreases from  $O(1)$  to  $O(\beta)$  as  $T^{-1}$ . Specifically, for  $T \sim \beta^{-1}$ , we have  $C_0 \sim \beta$  and  $S_0 \sim 1 - \frac{1}{2}\beta^2$ , from which the leading-order asymptotic forms

$$\partial_\eta F_0 \sim -\frac{1}{T}, \quad \partial_\eta^2 F_0 \sim -\frac{\beta}{T^3}, \quad \partial_\eta^4 F_0 \sim -\frac{9\beta}{T^5} \quad (4.4)$$

of all terms in (3.7) are readily determined. Hence, when  $T \sim \beta^{-1}$ ,  $F_0$  is of order  $O(\beta)$  and the series (4.1) is no longer asymptotic, and (3.7) must be rescaled using  $f_1 = \beta \mathcal{F}$  (where  $\mathcal{F} = O(1)$ ) and  $\tau = \beta T$  to give

$$\partial_\tau \mathcal{F} - \mathcal{F} \partial_\eta \mathcal{F} + \partial_\eta^2 (\partial_\eta^2 \mathcal{F} + \mathcal{F}) = 0. \quad (4.5)$$

Although an asymptotic analysis of (4.5) is not possible, numerical integrations indicate that  $|\mathcal{F}|_{\max}$  is a monotonically decreasing function of  $\tau$  for large  $\tau$ . Hence a further rescaling is introduced, namely  $\mathcal{F} = \epsilon \mathcal{G}$ , where  $\mathcal{G} = O(1)$  and  $0 < \epsilon \ll 1$ ; note that  $\epsilon$  is not necessarily related to  $\beta$ . Then, (4.5) rescales to

$$\partial_\tau \mathcal{G} - \epsilon \mathcal{G} \partial_\eta \mathcal{G} + \partial_\eta^2 (\partial_\eta^2 \mathcal{G} + \mathcal{G}) = 0. \quad (4.6)$$

The solution of (4.6) requires a two-time-scale expansion employing  $\tau_0 = \tau$  and  $\tau_1 = \epsilon^2 \tau$ : the ‘obvious’ slow time-scale  $\tau_1 = \epsilon \tau$  leads to a contradiction in the  $O(\epsilon)$

problem. Hence  $\partial_\tau = \partial_{\tau_0} + \epsilon^2 \partial_{\tau_1}$  in (4.6) is used together with the formal expansion

$$\mathcal{G}(\eta, \tau_0, \tau_1) = \sum_{n=0}^{\infty} \epsilon^n G_n(\eta, \tau_0, \tau_1). \quad (4.7)$$

Recalling the initial condition in (3.7), the  $\cos \eta$  spatial dependence gives the  $O(1)$  solution as

$$G_0(\eta, \tau_0, \tau_1) = A(\tau_1) \cos \eta,$$

with the corresponding  $O(\epsilon)$  solution readily determined as

$$G_1(\eta, \tau_0, \tau_1) = -\frac{1}{24} \{A(\tau_1)\}^2 (1 + g_1 e^{-12\tau_0}) \sin 2\eta,$$

wherein  $g_1$  is an arbitrary constant. In order to suppress secularity at order  $O(\epsilon^2)$ ,  $A(\tau_1)$  must satisfy the amplitude-evolution equation

$$\partial_{\tau_1} A = -\frac{1}{48} A^3 \quad \Rightarrow \quad A(\tau_1) = \{a_0 + \frac{1}{24} \tau_1\}^{-1/2},$$

wherein  $a_0$  is determined by matching at  $T = O(\beta^{-1})$ . Reverting to the original variables,  $f_1 \sim \beta \epsilon A(\epsilon^2 \beta T) \cos \eta$  gives

$$f_1(\eta, T) \sim \sqrt{\frac{24\beta}{T}} \cos \eta, \quad T \geq O(\beta^{-1}), \quad (4.8)$$

so that the amplitude of  $f_1$  divided by  $\beta$  is proportional to  $(\beta T)^{-1/2}$  at large times. By contrast, the first relationship in (4.4) indicates that, at early times,  $|f_1|/\beta \propto (\beta T)^{-1}$ . Note that the introduced arbitrary parameter  $\epsilon$  is absent, as required, from (4.8). Note also that, as  $\mathcal{G}$  decreases as  $\tau_1^{-1/2}$ , any further rescaling of (4.6) continues to give the asymptotic behaviour (4.8) for  $f_1$ . However, the  $T^{-1/2}$  decay eventually gives way to an exponential decay, as will be discussed in § 5*b*.

The behaviour predicted by the small- $\beta$  analysis is confirmed via the results portrayed in figure 3, which shows decaying  $|f_1|_{\max}/\beta$  plotted against  $\beta T$  where  $|f_1|$  is obtained from a numerical integration of the full KSE (3.7). Most notably, the gradient of the asymptotes clearly changes as predicted from  $-1$  to  $-\frac{1}{2}$  when  $\beta T = O(1)$ . For  $\beta < 0.01$ , curves join the  $T^{-1}$  asymptote before switching to the  $T^{-1/2}$  asymptote, whereas, for  $\beta > 0.1$ , curves head straight for the latter asymptote, taking several decades to arrive for the larger  $\beta$  values. That larger  $\beta$  values tend directly to the  $T^{-1/2}$  asymptote is entirely compatible with the analysis of § 5.

## 5. Large surface tension: the case $\beta \gg 1$

### (a) Algebraic amplitude decay

Shocks do not form when  $\beta \geq O(\gamma^{-1}) \gg O(1)$ , as per Hinch & Kelmanson (2003). The expectation of a gently decaying wave profile suggests the following two-time-scale expansion for the solution of (3.7):

$$f_1(\eta, T) = \sum_{n=0}^{\infty} \beta^{-n} \Phi_n(\eta, T_0, T_1),$$

where  $T_0 = T$  is the (slow) shock-formation time-scale and  $T_1 = \beta^{-1}T$  is an even slower time-scale. The  $O(1)$  solution is

$$\Phi_0(\eta, T_0, T_1) = -B(T_0, T_1) \cos \eta, \quad B(0, 0) = 1,$$

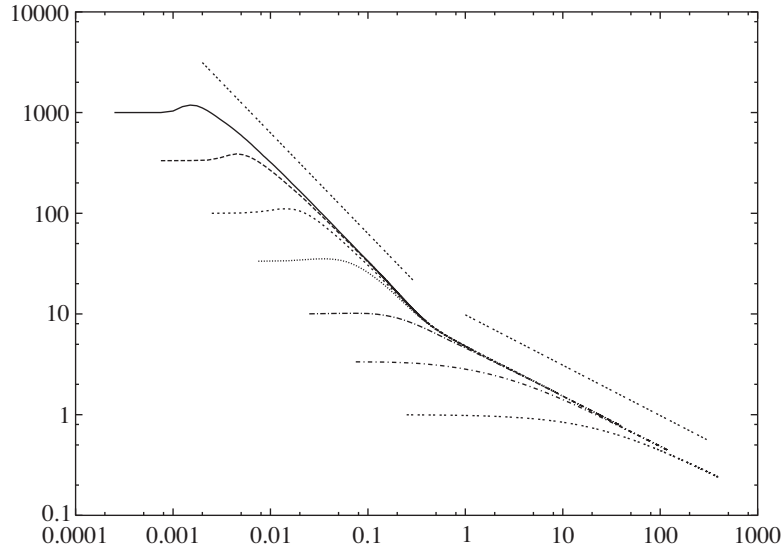


Figure 3. Log-log plot of  $|f_1|_{\max}/\beta$  against  $\beta T$  from numerical integrations of the KSE (3.7). Descending on the left-hand side of the figure,  $\beta$  takes the values  $1 \times 10^{-3}$ ,  $3 \times 10^{-3}$ ,  $1 \times 10^{-2}$ ,  $3 \times 10^{-2}$ ,  $1 \times 10^{-1}$ ,  $3 \times 10^{-1}$  and 1. The location of the ‘kink’ in the curves—which signifies the transition from the  $T^{-1}$  to  $T^{-1/2}$  decay—agrees well with the theoretical estimate of  $(\beta T, f_1/\beta) \sim (\pi^2/24, 24/\pi) \simeq (0.4112, 7.639)$ , although the numerical results suggest that the analysis of §4 requires  $\beta \ll 1 \times 10^{-1}$  rather than  $\beta \ll 1$ . For the smaller values of  $\beta$ , the early increase in  $f_1/\beta$  is attributable to the formation of capillary waves. The two straight lines correspond respectively to the theoretically obtained  $|f_1/\beta| = 2\pi/(\beta T)$  (upper) and  $|f_1/\beta| = 2\sqrt{24/(\beta T)}$  (lower), wherein the factor 2 has been included to translate the lines away from the (collapsed) numerical results.

and secularity is averted at order  $O(\beta^{-1})$  if  $\partial_{T_0} B \equiv 0$ , whence  $B = B(T_1)$  and

$$\Phi_1(\eta, T_0, T_1) = -\frac{1}{24} \{B(T_1)\}^2 \sin 2\eta.$$

In order to suppress secularity at order  $O(\beta^{-2})$ ,  $B(T_1)$  must satisfy the amplitude-evolution equation

$$\partial_{T_1} B = -\frac{1}{48} B^3, \quad B(0) = 1, \quad (5.1)$$

and hence

$$B(T) = \left\{ 1 + \frac{T}{24\beta} \right\}^{-1/2}. \quad (5.2)$$

Thus, for  $T \gg 1$ ,

$$f_1(\eta, T) \sim \sqrt{\frac{24\beta}{T}} \cos \eta, \quad T \geq O(\beta),$$

which should be contrasted with (4.8). The identical  $T^{-1/2}$ -asymptotic behaviours for both  $\beta \ll 1$  and  $\beta \gg 1$  are explained by noting that, when the amplitude  $A_1$  of  $f_1$  is small, the rescaling  $f_1 = A_1 \mathcal{F}$  ( $\mathcal{F} = O(1)$ ) and  $\tau = A_1 T$  in the KSE (3.7) gives

$$\partial_\tau \mathcal{F} - \mathcal{F} \partial_\eta \mathcal{F} + \frac{\beta}{A_1} \partial_\eta^2 (\partial_\eta^2 \mathcal{F} + \mathcal{F}) = 0, \quad (5.3)$$

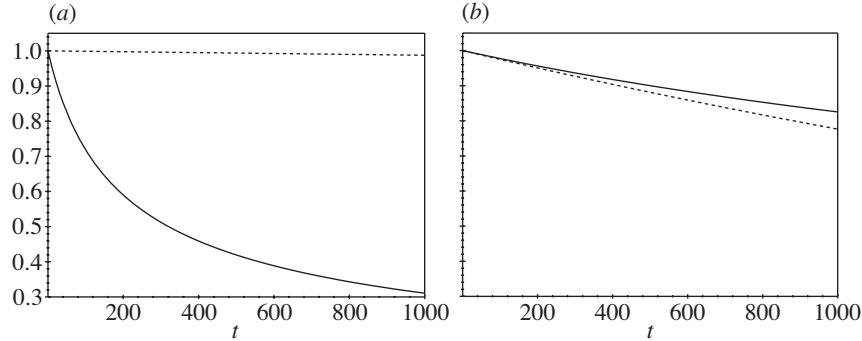


Figure 4. ———, Algebraic and - - - -, exponential amplitude decays of dominant perturbation (scaled with respect to  $\gamma$ ) in (5.4), from the steady state when  $\gamma = 0.05$  and (a)  $\alpha = \gamma^3/2$ , (b)  $\alpha = \gamma^2/2$ .

from which small  $A_1 (\ll \beta)$  and large  $\beta (\gg 1)$  are seen to be equivalent, admitting the same asymptotic forms. Moreover, (5.3) reveals a shock thickness of order  $O(\{\beta/A_1\}^{1/3})$ , which is  $O(\{\beta T\}^{1/3})$ , upon using the first expression in (4.4). Hence the shock which forms at  $T = 1$  disperses at  $T = O(\beta^{-1})$ , when the amplitude is  $O(\beta)$ ; thereafter,  $T^{-1/2}$  amplitude decay occurs irrespective of the magnitude of  $\beta$ .

(b) *Transition from algebraic to exponential amplitude decay*

Section 5a reveals that the amplitude of the  $O(\gamma)$  term in  $h$  decays as  $\{\gamma^3 t/24\}^{-1/2}$  when  $\beta \gg 1$ , i.e.  $\alpha \gg \gamma^3$ . However, when  $\alpha \gg \gamma^2$  (see (1.3)), Hinch & Kelmanson (2003) discover an exponential decay, specifically  $\exp(-81\alpha\gamma^2 t)$ . Therefore, as  $\beta$  is further increased, a third decay region (over and above  $(\gamma^3 t)^{-1}$  and  $(\gamma^3 t)^{-1/2}$ ) is encountered and, to determine the precise parameter regime of the transition between the  $(\gamma^3 t)^{-1/2}$  and  $\exp(-81\alpha\gamma^2 t)$  decays, note that, for small  $t$ , (5.2) and  $\exp(-81\alpha\gamma^2 t)$  can be expanded as

$$B(T) \simeq 1 - \frac{75\gamma^6}{4\alpha} t + \dots, \quad \exp(-81\alpha\gamma^2 t) \simeq 1 - 81\alpha\gamma^2 t + \dots, \quad (5.4)$$

respectively, so that transition from algebraic to exponential decay requires the small- $t$  balance  $\alpha \simeq \gamma^2/2$ , i.e. in keeping with  $\beta \gg 1$ . Thus, as  $\alpha$  is increased from  $O(\gamma^3)$  to  $O(\gamma^2)$ , one obtains not the algebraically decaying shock-like perturbations of the present work but the exponentially decaying low-harmonic perturbations in Hinch & Kelmanson (2003). Amplitude decay rates resulting from parameters spanning this transition region are shown in figure 4. Figure 4a explains the greater-than-expected large-time decay rates evident in figure 1c, d, and figure 4b demonstrates the long-term comparability (over a surprisingly large time-scale, given that the transition region was determined via small- $t$  expansions) of the negative-exponential and inverse-square-root decays when  $\alpha = O(\gamma^2)$ , providing strong corroboration of the transition region.

A more extensive view of the transition between the  $t^{-1/2}$  and exponential regimes can be obtained as follows. The algebraically and exponentially decaying amplitude  $A(t)$  expressed in terms of  $t$  satisfies

$$A_t = -\frac{75\gamma^6}{4\alpha} A^3 \quad \text{and} \quad A_t = -\frac{81\alpha\gamma^2}{1 + 144\alpha^2} A,$$

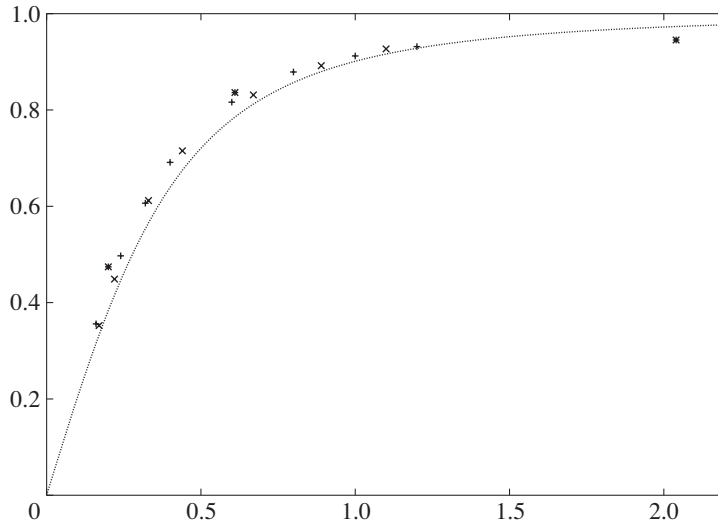


Figure 5. Large- $t$  transition factors  $\phi$  as a function of  $\alpha/\gamma^2$ , or  $5\delta/(6\sqrt{3})$ . The symbols are obtained by extracting the coefficient multiplying the exponential decay from numerical integrations of (1.2) with  $\gamma = 0.03$  ( $\times$ ),  $\gamma = 0.05$  ( $+$ ) and  $\gamma = 0.07$  ( $*$ ), and the continuous line is given by the limit in (5.6).

respectively, the former equation arising from (5.1) and the latter from eqns (3.8)–(3.10) of Hinch & Kelmanson (2003). Now consider  $A$  as the solution of a proposed ‘transition’ equation

$$A_t = -\frac{75\gamma^6}{4\alpha}A^3 - \frac{81\alpha\gamma^2}{1+144\alpha^2}A, \quad (5.5)$$

and approximate this by  $A_t \simeq -\nu A(\delta^{-2}A^2 + 1)$ , where  $\nu = 81\alpha\gamma^2$  and  $\delta = 6\sqrt{3}\alpha/(5\gamma^2)$ , so that  $\delta \ll 1$  and  $\delta = O(1)$ , respectively, correspond to algebraic and exponential decays. The solution of (5.5) with  $A(0) = 1$  is

$$A(t) = \{(1 + \delta^{-2})e^{2\nu t} - \delta^{-2}\}^{-1/2},$$

in which the large- $t$  transition factor—i.e. that multiplying the purely exponential decay  $\exp(-\nu t)$  of Hinch & Kelmanson (2003)—is therefore

$$\phi = \lim_{t \rightarrow \infty} \{1 + \delta^{-2}(1 - e^{-2\nu t})\}^{-1/2} = \frac{\delta}{(1 + \delta^2)^{1/2}} = \frac{\alpha}{\gamma^2} \left( \frac{\alpha^2}{\gamma^4} + \frac{25}{108} \right)^{-1/2}, \quad (5.6)$$

so that  $\lim_{\delta \rightarrow 0} \phi = 0$  and  $\lim_{\delta \rightarrow \infty} \phi = 1$ . Figure 5 shows a comparison between large- $t$  transition factors obtained numerically from (1.2) and the predicted value of  $\phi$  from (5.6), plotted as a function of  $\alpha/\gamma^2$ , i.e.  $5\delta/(6\sqrt{3})$ . Figure 5 both corroborates the small- $t$  estimate of  $\alpha/\gamma^2 \sim 1/2$  deduced via (5.4) and demonstrates the good agreement between numerical solutions and theory for a range of  $\gamma$  values, justifying that the heuristically proposed equation (5.5) does indeed capture the nature of the transition. The justification lies in the fact that the algebraic and exponential secular perturbations are independent, arising in different regions of parameter space, and so their leading-order effects may simply be added. Since  $\beta \gg 1$  when  $\alpha = O(\gamma^2)$ , by the discussion of (5.3),  $\alpha = O(\gamma^2)$  corresponds to small amplitude  $A_1$ ; specifically

$A_1 \ll \beta$ . Hence, the transition from  $T^{-1/2}$  to exponential decay also occurs when  $A_1 \ll \beta \ll 1$ , i.e. the combination of small  $\beta$  and small amplitude admits an exponential decay, as noted at the end of § 4. A summary of all possible decay transitions, with particular emphasis upon realizable observations based upon physical data, is presented in § 7.

## 6. Quasi-steady shock structure

The implicit solution (4.3) of the KSE (3.7) applies outside the thin shock region which forms at  $\eta = \pi/2$ . Retaining only the highest derivative for the purposes of the inner scaling, the quasi-steady shock solution  $f(x)$ , where  $x = \eta - \pi/2$ , therefore satisfies

$$-f\partial_x f + \beta\partial_x^4 f \simeq 0, \quad (6.1)$$

which can be integrated once to give

$$f^2 - A_s^2 = 2\beta\partial_x^3 f, \quad (6.2)$$

wherein  $A_s$  is the shock amplitude. Then, the transformations

$$f = A_s \hat{f} \quad \text{and} \quad x = \left(\frac{2\beta}{A_s}\right)^{1/3} \hat{x} \quad (6.3)$$

(cf. discussion on shock thickness immediately following (5.3)) reduce (6.2) to the canonical form

$$\hat{f}^2 - 1 = \partial_{\hat{x}}^3 \hat{f}, \quad (6.4)$$

which is solved numerically using MAPLE9† by shooting from  $\hat{x} = 0$ , with  $\hat{f}(0) = \partial_{\hat{x}}^2 \hat{f}(0) = 0$ , such that  $\hat{f}(\hat{x}) \rightarrow \pm 1$  as  $\hat{x} \rightarrow \pm\infty$ ; the value  $\partial_{\hat{x}} \hat{f}(0) \simeq 1.060\,765\,34$  is required. We note that, in considering the closely related rimming-flow problem, Ashmore *et al.* (2003) also employ (their eqn (3.8)) a scaling of  $O(\alpha^{1/3})$ , as per the second equation in (6.3), to show that  $H$ , the *steady* film thickness non-dimensionalized with respect to the flux, satisfies the Landau–Levich–Derjaguin equation  $H^3 H''' + H = 1$ ; however, their scaling dependence on  $\gamma$  is different from that presently employed.

In order to effect a comparison between the quasi-steady-shock solution  $\hat{f}$  of the canonical (6.4) and the shock-like solutions of (1.2), the transient disturbance in the solution of (1.2) must be isolated and scaled appropriately. To this end, (3.1)–(3.5) together yield

$$h(\theta, T) = 1 + \gamma(\cos \theta + f_1(\eta, T)) + \gamma^2\left(\frac{3}{2} \cos 2\theta + H_2(\xi, \eta, T)\right) + O(\alpha\gamma^2, \gamma^3). \quad (6.5)$$

Denoting by  $\tilde{h}$  the numerical solution of (1.2), and by  $\tilde{A} = \tilde{A}(T)$  the theoretical amplitude (determined by (4.3)) of the decaying transient  $f_1$ , (6.5) implies that

$$\tilde{H}(\theta, T) \equiv \frac{\tilde{h}(\theta, T) - 1 - \gamma \cos \theta - \frac{3}{2}\gamma^2 \cos 2\theta}{\gamma\tilde{A}} = \frac{f_1(\eta, T)}{\tilde{A}} + O\left(\frac{\gamma}{\tilde{A}}\right). \quad (6.6)$$

† Using both polynomial and Burlirsch–Stoer rational extrapolation in Gear’s one-step method in the function `dsolve`, with relative error, absolute error and initial  $\Delta\hat{x}$  all equal to  $1.0 \times 10^{-8}$ , and a minimum  $\Delta\hat{x}$  of  $1.0 \times 10^{-11}$ .

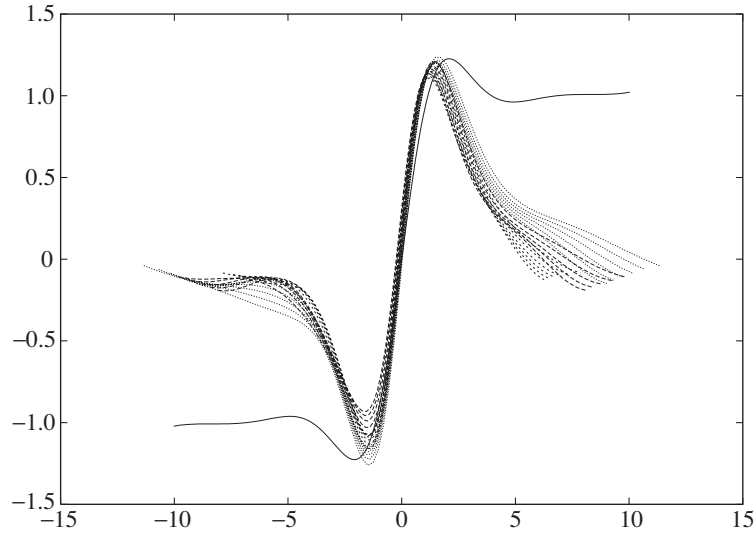


Figure 6. Plots of theoretical quasi-steady shock  $\hat{f}(\hat{x})$  (solid curve) and scaled numerically determined transients  $\tilde{H}(\tilde{\theta}, T)$ , in which  $\gamma$ ,  $\alpha$  and  $\beta$  are respectively:  $8.0 \times 10^{-2}$ ,  $1.0 \times 10^{-4}$  and  $6.5104 \times 10^{-3}$  (dotted curves);  $1.0 \times 10^{-1}$ ,  $3.0 \times 10^{-4}$  and  $1.0 \times 10^{-2}$  (long-dashed curves);  $8.0 \times 10^{-2}$ ,  $3.0 \times 10^{-4}$  and  $1.953 \times 10^{-2}$  (short-dashed curves). The horizontal scale is common to both  $\hat{x}$  and  $\tilde{\theta}$ . The ‘fanning’ of the scaled numerical transients is explained in the text.

Rescaling the independent variables via

$$\theta = \left(\frac{2\beta}{\tilde{A}}\right)^{1/3} \tilde{\theta} \quad \text{and} \quad \eta = \frac{\pi}{2} + \left(\frac{2\beta}{\tilde{A}}\right)^{1/3} \tilde{x}, \quad (6.7)$$

the function  $\tilde{H}(\tilde{\theta}, T)$  obtained via the definition in (6.6) therefore approximates the normalized solution  $f_1(\tilde{x}, T)/\tilde{A}$  of the KSE (3.7), which, by the first scaling in (6.3), may be compared directly with the quasi-steady solution  $\hat{f}(\hat{x})$  of (6.4).

$\tilde{H}(\tilde{\theta}, T)$  is determined by first solving numerically the full governing equation (1.2) for  $\tilde{h}(\tilde{\theta}, T)$  using a finite-difference method which is fourth-order in space and first-order (explicit) in time, using 50 equally spaced points in  $0 < \tilde{\theta} < 2\pi$ . Plots are captured at times when the slope at the origin,  $\tilde{h}_{\tilde{\theta}}(0, T)$ , takes its first maximum just after  $T = 30\gamma^3 t \simeq 4, 5, 6, 7, 8, 9$  (e.g. at  $T = 4.052, 5.071, 6.089, 7.108, 8.126$  and  $9.144$  in the case  $\gamma = 8.0 \times 10^{-2}$  and  $\alpha = 1.0 \times 10^{-4}$  (i.e.  $\beta = 6.5104 \times 10^{-3}$ )). This criterion is chosen since, for small surface tension ( $\alpha \ll 1$ ), the steady state is symmetric/even about  $\tilde{\theta} = 0$ , so that when the slope is the maximum the shock wave should be centred on  $\tilde{\theta} = 0$  (cf. the first scaling in (6.7)). To find the theoretical amplitude  $|f_1(\eta, T)|_{\max}$  of the decaying transient at the specified time  $T$ , the characteristic solution of (4.2),  $F_0 = -\cos \eta_0$ , where  $\eta_0$  is the solution of  $\eta_0 + T \cos \eta_0 = \eta$ , is used.

An inspection of unscaled results in the case  $\gamma = 8.0 \times 10^{-2}$ ,  $\alpha = 3.0 \times 10^{-4}$  (i.e.  $\beta = 1.953 \times 10^{-2}$ ) reveals that the amplitude of the transient decays by the factor 0.471 in between  $T = 4.050$  and  $T = 9.143$ , and the theoretical factor based on the solution of (4.2) is 0.505; both figures confirm the prediction of  $1/T$  decay (which gives the exact factor 0.443). It is noteworthy that the  $1/T$  decay is evident well before the asymptotic  $T \gg 1$  regime.

Table 1. *The four theoretically possible decay sequences*

(Phases 1, 2 and 3 correspond respectively to initial decay, subsequent low-amplitude decay and ultimate asymptotic decay.)

sequence	conditions	phase 1	phase 2	phase 3
I	$\alpha > \gamma^2/2$	exponential	exponential	exponential
IIa	$\alpha < \gamma^2/2, \beta \gg 1$	$t^{-1/2}$	exponential	exponential
IIb (i)	$\alpha < \gamma^2/2, \beta \ll 1, \gamma > 1/60$	$t^{-1}$	exponential	exponential
IIb (ii)	$\alpha < \gamma^2/2, \beta \ll 1, \gamma < 1/60$	$t^{-1}$	$t^{-1/2}$	exponential

Figure 6 shows a comparison between the theoretical shock solution  $\hat{f}(\hat{x})$  and the numerically determined transients  $\tilde{H}(\tilde{\theta}, T)$ , the latter for a range of values of  $\gamma$  and  $\alpha$ . By construction, the quasi-steady shock curve and the transient curves for different times should almost be superposed, the  $O(\gamma/\tilde{A}(T))$  error in (6.6) precluding exact superposition. Furthermore,  $\hat{x}$  and  $\tilde{\theta}$  admit only *approximately* the same scaling, since the former uses the fixed amplitude  $A_s$  in (6.3), whereas the latter uses the slowly decreasing amplitude  $\tilde{A}(T)$  which, via (6.7), gives the slow (horizontal) ‘fanning’ of the  $\tilde{H}(\tilde{\theta}, T)$  curves towards the centre of figure 6. For example, the rightmost abscissae on the dotted curves compress by a factor of approximately 0.796 (i.e. from  $\tilde{\theta} = 11.341$  down to  $\tilde{\theta} = 9.030$ ) in between  $T = 4.052$  and  $T = 9.144$ ; this figure agrees well with the  $1/T$ -decay-based theoretical compression of  $(4.052/9.144)^{1/3} = 0.762$ .

The superposition is best in the vicinity of the origin, where the slope and the main rise of the shock (for  $|\tilde{\theta}| < 1.5$ ) agree well. For the lower values of surface tension (dotted curves) the maximum height agrees extremely well with the theoretical solution (solid line), which has a maximum of  $\hat{f} = 1.226857$  when  $\hat{x} = 2.07955$ . Outside the main rise, however, the amplitude of the scaled transient solutions is considerably smaller than that of the theoretical shock because, in the cases studied, the shock-amplitude decay was accompanied by a thickening of the shock (not immediately evident due to the scaling in figure 6) to between 10% (at  $T \simeq 4$ ) and 20% (at  $T \simeq 9$ ) of the whole interval.

## 7. Decay transition sequences and their observability

Three distinct amplitude decay rates have been discovered and the transitions between them discussed in general terms. First, figure 3 and the discussion thereon considers the transition between the  $T^{-1}$  decay of §4 and the  $T^{-1/2}$  decay of §5, then figure 5 summarizes the transition between the  $T^{-1/2}$  decay and the exponential decay analysed by Hinch & Kelmanson (2003). Depending on the relative magnitudes of  $\gamma$ ,  $\alpha$  and  $\beta$ , a number of decay sequences may arise.

Note from table 1 that the overall condition  $\gamma \ll 1/60$  must apply if sequence IIa is to be observed in practice. Whether or not this condition—and, indeed, any other condition in table 1—is realistic can be determined from the information in table 2, which enables determination of  $\alpha/\gamma^2$ ,  $\beta$  and  $\gamma$  when the radius  $a$ , angular velocity  $\omega$  and film thickness  $h$  are prescribed. The information, for five different fluids at 100 KPa and 288 K, is based upon the physical data (in SI units) at <http://imartinez.etsin.upm.es/dat1/eLIQ.htm>, together with a value of  $g = 9.81 \text{ m s}^{-2}$ .

Table 2. Values of parameter combinations in table 1, based upon physical data (see text), for a film of thickness  $h$  on a cylinder of radius  $a$  rotating with angular velocity  $\omega$

(This information can be used to determine experimental  $(h, a, \omega)$  combinations admitting the theoretically possible decay sequences of table 1.)

fluid	$\frac{ha^2}{\omega} \frac{\alpha}{\gamma^2}$	$\frac{h^3 a}{\omega^2} \beta$	$\frac{\omega a}{h^2} \gamma$
water	$2.28 \times 10^{-12}$	$2.33 \times 10^{-20}$	$3.26 \times 10^6$
ethylene glycol	$2.43 \times 10^{-11}$	$4.47 \times 10^{-18}$	$1.81 \times 10^5$
glycerine	$1.73 \times 10^{-9}$	$1.96 \times 10^{-14}$	$2.94 \times 10^3$
silicone oil DMS-10	$6.89 \times 10^{-12}$	$7.02 \times 10^{-19}$	$3.27 \times 10^5$
mercury	$1.29 \times 10^{-13}$	$1.51 \times 10^{-21}$	$2.86 \times 10^7$

For all fluids (i.e. not just those referenced in table 2), sequence *I* of table 1 can at first sight be achieved by making the film thickness sufficiently small. However, it is to be borne in mind that the lubrication approximation (1.2) ceases to be valid as van der Waals effects dominate in the limit  $h \rightarrow 0$ , i.e. solutions in which  $h$  is of the order of a fraction of a micrometre should be rejected. To illustrate this, consider an example with  $a$  fixed at 1 cm. Taking  $\alpha/\gamma^2 = 1 > 1/2$ , an angular velocity of  $\omega = 20\pi$  gives  $h = 1.09$  mm for glycerine and  $h = 1.43$   $\mu$ m for water; to sustain a water film of thickness 1.43 mm would therefore require an angular velocity of  $\omega = 20\,000\pi$ . It is inferred that sequence *I* would be observable for glycerine but not for water. If  $\gamma = \frac{1}{600} \ll \frac{1}{60}$ ,  $a = 10^{-2}$  and  $\omega = 20\pi$ ,  $h = 0.596$  mm for glycerine and  $h = 17.9$   $\mu$ m for water. Hence, sequence *IIa* would be observable for the former but not for the latter unless, as above,  $\omega$  were increased by a factor of 1000. Finally, if  $\beta = 1/10 \ll 1$ ,  $a = 10^{-2}$  and  $\omega = 20\pi$ ,  $h = 4.26$  mm for glycerine and  $h = 0.14$  mm for silicone oil DMS-10; both are perfectly reasonable from an experimental viewpoint. However,  $\gamma = 0.0851 > \frac{1}{60}$  for glycerine and  $\gamma = 0.0103 < \frac{1}{60}$  for silicon oil DMS-10, so that the former and latter respectively admit the *IIB*(i) and *IIB*(ii) decay sequences. It is concluded that all of the four discovered decay sequences are observable in practice.

## References

- Ashmore, J., Hosoi, A. E. & Stone, H. A. 2003 The effect of surface tension on rimming flows in a partially filled rotating cylinder. *J. Fluid Mech.* **479**, 65–98.
- Frigo, M. & Johnson, S. G. 1998 FFTW: an adaptive software architecture for the FFT. In *Proc. IEEE Int. Conf. on Acoustics, Speech and Signal Processing, Seattle*, vol. 3, pp. 1381–1384. New York: IEEE Press.
- Hinch, E. J. & Kelmanson, M. A. 2003 On the decay and drift of free-surface perturbations in viscous, thin-film flow exterior to a rotating cylinder. *Proc. R. Soc. Lond. A* **459**, 1193–1213.
- Holmes, M. H. 1995 *Introduction to perturbation methods*. Springer.
- Moffatt, H. K. 1977 Behaviour of a viscous film on the outer surface of a rotating cylinder. *J. Méc.* **187**, 651–673.
- Pukhnachev, V. V. 1977 Motion of a liquid film on the surface of a rotating cylinder in a gravitational field. *Z. Prikl. Mekh. Tekh. Fiz.* **3**, 78–88. (English transl. 1977 *J. Appl. Mech. Tech. Phys.* **18**, 344–351.)